ELSEVIER

Polymer 41 (2000) 8833–8837

polymer

www.elsevier.nl/locate/polymer

Modeling polymer crystallization from solutions

M. Muthukumar*, P. Welch

Polymer Science and Engineering Department, Materials Research Science and Engineering Center, University of Massachusetts, Amherst, MA 01003, USA

Received 20 October 1999; received in revised form 15 February 2000; accepted 18 February 2000

Abstract

In an effort to understand early-stage polymer crystallization and the recently proposed spinodal mode of crystallization, we have performed Brownian dynamics simulations of crystallizing polymer chains. We find that the mechanism of polymer crystallization is nucleation and growth even in the induction period, although scattering data can be superficially fitted to the spinodal decomposition description. The microscopic model used in our simulations reveals rich details of the kinetic pathway of polymer crystallization in very early stages. © 2000 Elsevier Science Ltd. All rights reserved.

Keywords: Polymer crystallization; Spinodal mode; Microscopic model

1. Introduction

Recent time-resolved scattering experiments [1–7] are able to probe polymer crystallization kinetics at very early times. These investigations have revealed that formation of sufficiently well-ordered crystalline domains is preceded by density fluctuations reminiscent of spinodal decomposition in polymer blends. The claim [8] that spinodal decomposition into two liquid phases occurs at early times prior to the formation of crystalline nuclei in a one-component polymer system is intriguing. Furthermore, although the phenomenological theory of Lauritzen and Hoffman [9,10] is quite successful in parameterizing various experimentally observed growth laws, a theory of polymer crystallization based on a microscopic description is desirable, as indicated by the wealth of other theoretical studies [11–14] to this end.

Motivated by these considerations, we have performed Brownian dynamics simulations of polymer crystallization from solution. We have modeled the polymer crystallization by following the competition between the attraction among non-bonded monomers and the torsional energies along the chain backbone. In addition to monitoring the rich details of the crystallization process, these simulations exhibit many experimental observations previously reported in the literature, such as the inverse relation between lamellar thickness and degree of undercooling, quantized kinetics of lamellar thickening, and molecular fractionation at the growth front. In addition, the present simulations offer an explanation of the recently claimed "spinodal mode" of polymer crystallization without invoking spinodal decomposition.

2. Simulation method

The simulation model attempts to incorporate just enough detail to observe chain-folding without impeding the efficiency of the simulation. As a result, the united atom model for polyethylene is chosen for a polymer chain, in which each methylene unit is treated as a bead in a bead-spring model. Typical chain lengths, N, in our simulations range from 500 to 10,000 united atoms. The force field parameters are modeled after the paper by Paul et al. [15], which are in close agreement with experimental measurements on the polyethylene melt. Those parameters are slightly modified in our model to enhance computational efficiency: the terminal methyl groups have the same force field parameters as the methylene units, the chain torsional stiffness is higher, and the bonds are more flexible. Similar computer simulation approaches have recently appeared in the literature [16–19].

The total potential energy consists of the potential energy of each bond arising from bond stretch U_r, bond angle U_θ, and bond torsion U_ϕ, and non-bonded bead–bead interaction which is taken to be the Lennard-Jones interaction $U_{\text{L-J}}$. The potential energy associated with bond stretch is taken to be

$$U_r = k(r - r_0)^2$$

* Corresponding author.
E-mail address: muthu@kali.pse.umass.edu (M. Muthukumar).

PII: S0032-3861(00)00226-3

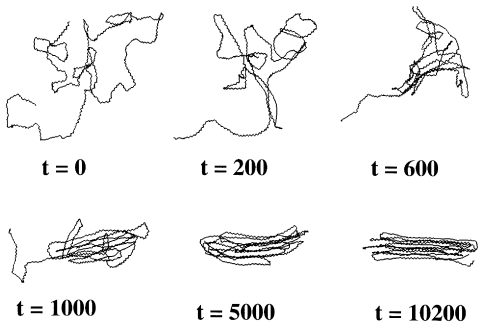

Fig. 1. Primary nucleation sequence. Snapshots for $N = 700$ shown.

where r is the bond length and r_0 is the equilibrium bond length. The spring constant k is taken to be 115 kcal/mol Å^2 and $r_0 = 1.54$ Å. The potential energies associated with bond angle θ and torsion angle ϕ are assumed to be of the form

$$U_\theta = k_\theta(\cos\theta - \cos\theta_0)^2$$

and

$$U_\phi = k_1(1 - \cos\phi) + k_2(1 - \cos 2\phi) + k_3(1 - \cos 3\phi)$$

where $\theta_0 = 109°$; $k_\theta = 60.0$, $k_1 = 3.02$, $k_2 = -0.560$, and $k_3 = 2.58$ kcal/mol. The Lennard-Jones potential $U_{\text{L-J}}$ is

$$U_{\text{L-J}} = \epsilon[(\sigma/r)^{12} - 2(\sigma/r)^6]$$

where the interaction strength ϵ is set to 0.112 kcal/mol. The equilibrium distance σ is 4.53 Å for beads further than five repeat units apart along the chain backbone. In order to enhance computational stability, beads that are closer than five repeat units along the chain interact with a σ value equal to 1.54 Å. This is expected to have little effect on the behavior of the chain other than slightly increasing the chain's local flexibility. However, the stiff torsional constraint overwhelms this enhancement. The Lennard-Jones potential contains a coefficient of 2 for the attractive part so that the minimum of this potential occurs at $r = \sigma$.

For the actual computation, reduced units are used throughout and all data presented here are expressed in terms of the reduced units. The units have been renormalized to a united-atom mass m of 1, an equilibrium bond length r_0 of 1, and a Lennard-Jones ϵ of 1. Thus, the reduced temperature, T^*, is equal to $k_B T/\epsilon$, the reduced energy is E/ϵ and the reduced time is $t\sqrt{\epsilon/m\sigma^2}$.

The magnitude of the force field parameters shows that the bond length and the bond angle are basically rigid, and the torsional angle changes the most during the simulation. We have found that the exact choices of bond length stiffness and bond angle stiffness are unimportant as long as they are high relative to the torsional angle parameters.

The equations of motion are integrated according to the methodology of Langevin dynamics [20,21]. In Langevin dynamics, the motion of the particles is described by the Langevin equation (Eq. (1)) which consists of inertial terms, force field, frictional drag, and noise, respectively [20,21].

$$\ddot{r}_i = -\nabla U_i - \Gamma\dot{r}_i - W_i(t) \tag{1}$$

The Langevin dynamics method simulates the effect of individual solvent molecules through the noise W, which is assumed to be Gaussian. The friction coefficient Γ is related to the autocorrelation function of W through the fluctuation–dissipation theorem,

$$\langle W_i(t)\cdot W_j(t')\rangle = \delta_{ij}\delta(t - t')6k_B T\Gamma \tag{2}$$

Furthermore, we set Γ to be 1, between the over-damped regime and the purely deterministic regime. We use the velocity Verlet finite-differencing scheme [21,22] for integration. This scheme, at larger time steps, is comparable in accuracy to the Gear predictor–corrector algorithms [23], but requires less memory and is simpler in implementation. In the velocity Verlet algorithm, the velocities of the particles are calculated at every half time step, leading to greater accuracy. The time step used in the data presented here is 0.004. Since in Langevin dynamics the effect of the solvent is implicit, we can only estimate the relationship between simulation time and real time. Due to the coarse-grained nature of the united-atom model, the time unit is expected to be longer than that of an atomistic model, on the order of monomeric relaxation time rather than atomic relaxation time. Based on the example of liquid argon [24], the relaxation time for a typical solvent molecule is of the order of 10^{-12} s. We therefore expect the relaxation time of the united atom to be also of the order of 10^{-12} s. Since in each iteration of a Langevin dynamics simulation the noise is uncorrelated and the time step is 0.004, one time unit in our simulation is on the order of 10^{-10} s. The precise relationship between the time unit used in the Langevin dynamics simulations performed here and the actual time is not yet established. Throughout the simulations, data are collected at periodic intervals. These include the radii of gyration, the kinetic and potential energies, and the spherically averaged single particle form factor, $S(\vec{q})$, calculated as

$$S(\vec{q}) = \frac{1}{N^2}\sum_{i=1}^{N}\sum_{j=1}^{N}\frac{\sin(\vec{q}\cdot\vec{r}_{ij})}{\vec{q}\cdot\vec{r}_{ij}} \tag{3}$$

where

$$|\vec{q}| = \frac{4\pi}{\lambda}\sin\left(\frac{\theta}{2}\right) \tag{4}$$

3. Results and discussion

The first step in our study is the determination of the melting temperature for our model chains. We create a random initial configuration and equilibrate it at $T^* = 15.0$. Then, we quench the chain to $T^* = 10.0$ and allow crystallization to take place. Once a single chain-folded structure is obtained, we perform several runs at heating

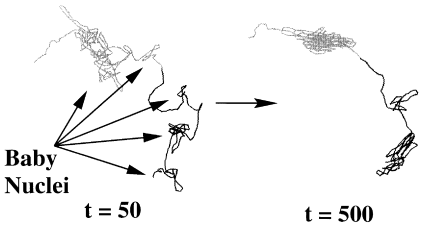

Fig. 2. Typical chain conformational evolution in the early stages of crystallization. Snapshots for $N = 2000$ shown.

rates ranging from 0.0001 to $0.002T^*$/time units. Discontinuities are observed in the slopes of both the total potential energy and global order parameter at the onset and ending of melting. The equilibrium melting temperature is estimated by extrapolation of the observed melting temperatures to zero heating rate. This temperature is approximately $T^* = 11.0 \pm 0.2$.

After determining the melting temperature as outlined above, we proceed to study the primary nucleation in which a chain folds into a lamellar crystal. As reported in Ref. [25], Fig. 1 shows a typical sequence of images depicting this event and the values of time are indicated in the frames. A chain of $N = 700$ beads is equilibrated above the melting point ($T^* = 12.0$) and quenched to $T^* = 9.0$. As another example, in Fig. 2, a chain of $N = 2000$ beads is equilibrated above the melting point ($T^* = 20.0$) and quenched to $T^* = 9.0$. The time steps shown in the sequence are selected from representative configurations during the course of crystallization. As seen in Figs. 1 and 2, several regions of segmental aggregation with some visibly apparent local orientational order are formed, connected by the same single chain. We refer to these regions as "baby nuclei". The strands connecting these baby nuclei are flexible with considerable configurational entropy. As time progresses, the monomers in the flexible strands are reeled into the baby nuclei while the orientational order in each nuclei increases. Simultaneously, the competition between nuclei for further growth dissolves some nuclei. Thus, the description is essentially the same as nucleation and growth encountered in small molecular systems, except that the polymer now is long enough to participate in several nuclei. Similar regions as our "baby nuclei" composed of segments from different chains have also been observed in simulations of the "melt" state of oligomers [19].

We observe that the average distance between baby nuclei does not change during this interval. But the number of monomers in the connectors is reduced accompanied by an increase in segmental orientation inside the nuclei as time increases. To quantify this result, we plot in Fig. 3 the difference in the structure factor $S(\vec{q}, t)$ at time t and the initial structure factor $S(\vec{q}, 0)$. As seen in experiments [1–7], we observe a scattering peak at $\vec{q}_{\max}$. In our simulations, we find $\vec{q}_{\max}$ to correspond to the spacing between baby

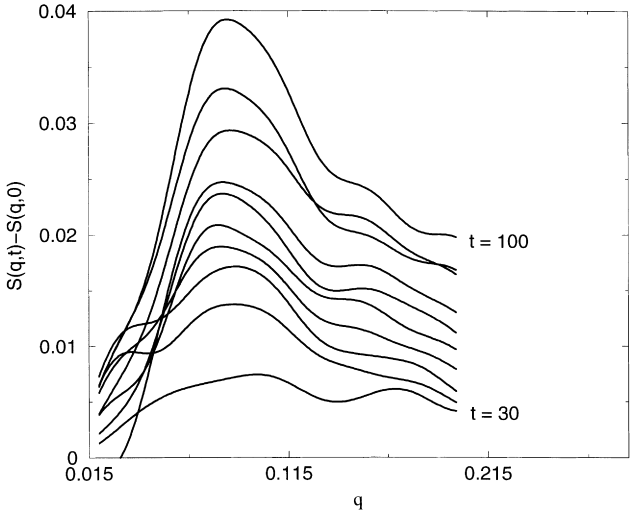

Fig. 3. Typical scattering behavior in the early stages of crystallization. Data for $N = 2000$ shown.

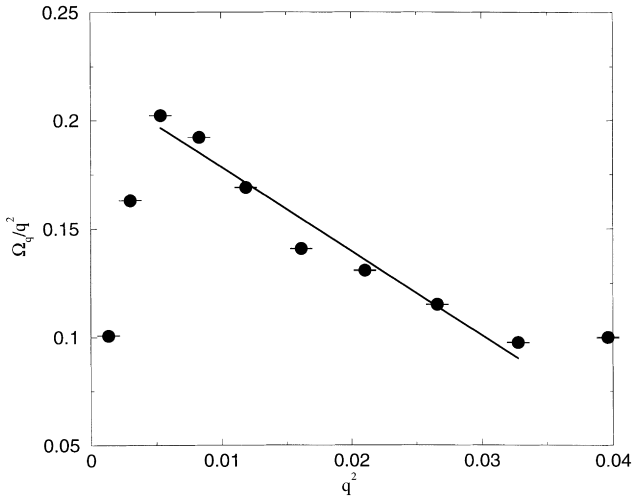

Fig. 4. Fluctuation growth rates as a function of q^2. Data for $N = 2000$ shown.

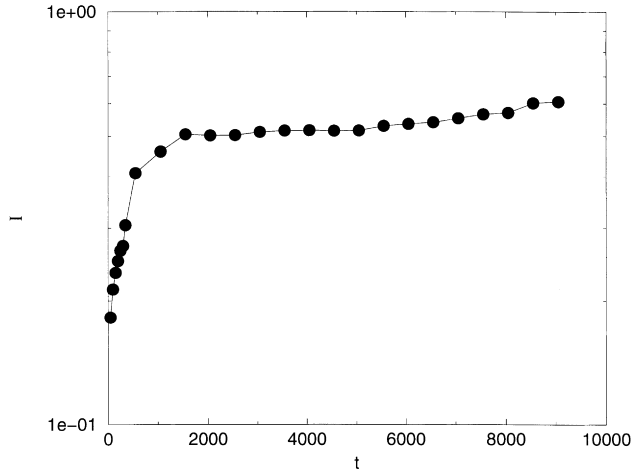

Fig. 5. Total scattering intensity as a function of time. Data for $N = 2000$ shown.

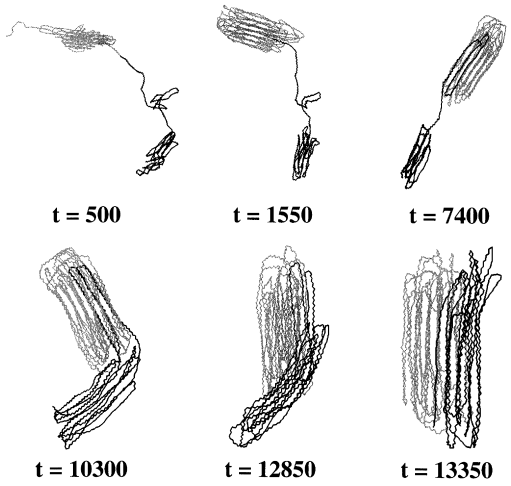

Fig. 6. Typical chain conformational evolution spanning time from the early stages to the terminal stages of crystallization. The homopolymer chain is partially shaded to illustrate movement of chain segments into the crystalline domains. Snapshots for $N = 2000$ shown.

nuclei and the peak position to be essentially independent of time in the early stages. Fig. 4 contains a plot of Ω_q/q^2 versus q^2, where Ω_q is the rate of growth of fluctuations with wave vector $\vec{q}$. According to the linearized theory of spinodal decomposition for mixtures, $S(\vec{q},t) \propto \exp(2\Omega_q t)$, where $\Omega_q \propto q^2(1 - Bq^2)$ with B being a positive constant. Therefore, a plot of Ω_q/q^2 versus q^2 must be linear with a negative slope if spinodal decomposition is present. Experimentalists have used this criterion to claim that spinodal decomposition is the mechanism of polymer crystallization at the early stage. As in experiments, we also observe that Ω_q/q^2 versus q^2 is linear with a negative slope. However, this is not an evidence for spinodal decomposition because this behavior is observed for intermediate values of $\vec{q}$. Our results show that for small $\vec{q}$, $\Omega_q \propto q^4$, in agreement with experiments but in disagreement with the predictions of spinodal decomposition.

The time-dependence of the total integrated intensity I is plotted in Fig. 5. For early times, $\ln I$ is linear in time. At later times ($t \geq 1000$), I grows very slowly with time. All of these features are seen in experiments [1–7]. To get more insight into this process, we present typical configurations at various times in Fig. 6 ($t = 500$, 1550, 7400 10300, 12850, 13350). For the sake of clarity, we have used two shades for the polymer although the chain is a homopolymer. As pointed out already, monomers in the connectors are transferred into the growing nuclei in the very early stage. This process continues until the connector is essentially stretched out while keeping the average inter-nuclei distance the same. Then the connector is pulled into the nuclei to varying degrees until the nuclei impinge against each other. This is followed by a cooperative reorganization by which nuclei merge to form a single lamella. The mechanism of the merger is not by sequentially placing stems, but by a highly cooperative process involving all stems of the lamella.

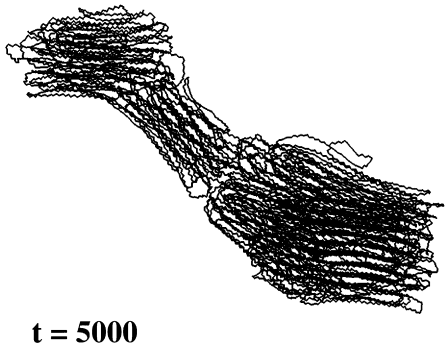

Fig. 7. Typical chain conformation for $N = 10\,000$ displaying lamella frustration.

The merging of the nuclei can take long times depending on chain length. As an example, Fig. 7 shows the configuration of a chain with $N = 10000$ at $t = 5000$ undergoing crystallization at $T^* = 9.0$. Now the time taken for the cooperative rearrangement of the three nuclei to form one lamella is very long. In fact, we find the structure to be essentially static at the average configuration of Fig. 7 even at later times. It is hoped that our planned simulations for large systems will lead to an understanding of the relationship between such kinetically frustrated [28] metastable structures and the onset of lamellar branching in the context of spherulites.

4. Conclusions

The Brownian dynamics simulations presented here show that the mechanism of polymer crystallization at very early stages is actually nucleation and growth, although the scattering data can be superficially fitted to spinodal decomposition. The key feature that distinguishes polymers from small molecules at early stages of crystallization is that in the case of polymers, a single chain can participate in several nuclei. Although our observations are made for crystallization from solutions whereas the experiments are for melt-crystallized polymers, the essential features of the simulation results reported here are seen [25] for many chains also. We plan to simulate very high polymer concentrations in the future. We must also point out that structures similar to our baby nuclei composed of segments from different chains have been observed in simulations of the "melt" state of oligomers [19]. Based on our extensive simulation results underway, we believe that the primordial stage of polymer crystallization is similar in both solution and melt grown lamellae. We have previously reported [25] our simulation results on: (i) the dependence of lamellar thickness Λ on quench depth ΔT^*, with $\Lambda = (C_1/\Delta T^*) + C_2$, where C_1 and C_2 are constants without any catastrophe, in agreement with experiments [26]; (ii) crystallization at a growth front as a function of commensurability between the thickness of the growth front and the length of the crystallizing

chains; and (iii) the kinetic pathway of lamella thickening as stepwise and quantized in agreement with experiments [27]. The interested reader should refer to Ref. [25].

Finally, we must point out that the quality of the chosen potentials in our simulations plays a crucial role in adequately describing various experimental systems. Much more work is necessary before our simulations can represent a particular experimental system. Nevertheless, we believe that the essential features of polymer crystallization are captured in our simulations.

Acknowledgements

Acknowledgment is made to NSF Grant no. DMR 9970718 and to the Materials Research Science and Engineering Center at the University of Massachusetts.

References

[1] Imai M, Mori K, Mizukami T, Kaji K, Kanaya T. Polymer 1992;33:4451.
[2] Imai M, Mori K, Mizukami T, Kaji K, Kanaya T. Polymer 1992;33:4457.
[3] Imai M, Kaji K, Kanaya T. Phys Rev Lett 1993;71:4162.
[4] Imai M, Kaji K, Kanaya T. Macromolecules 1994;27:7103.
[5] Imai M, Kaji K, Kanaya T, Sakai Y. Phys Rev B 1995;52:12 696.
[6] Ezquerra TA, Lopez-Cabarcos E, Hsiao BS, Balta-Calleja FJ. Phys Rev E 1996;54:989.
[7] Terrill NJ, Fairclough PA, Towns-Andrews E, Komanschek BU, Young RJ, Ryan AJ. Polymer 1998;39:2381.
[8] Olmsted PD, Poon WCK, McLeish TCB, Terrill NJ, Ryan AJ. Phys Rev Lett 1998;81:373.
[9] Hoffman JD, Davies GT, Lauritzen JI. Treatise on solid-state chemistry, vol. 3. New York: Plenum Press, 1976.
[10] Hoffman JD, Miller RL. Polymer 1997;38:3151.
[11] Point JJ. Macromolecules 1979;12:770.
[12] Sadler DM, Gilmer GH. Phys Rev Lett 1986;56:2708.
[13] Doye JPK, Frenkel D. J Chem Phys 1999;110:7073.
[14] Armitstead K, Goldbeck-Wood G. Advances in polymer science, vol. 100. New York: Springer, 1992.
[15] Paul W, Yoon DY, Smith GD. J Chem Phys 1995;103:1702.
[16] Kavassalis TA, Sundararajan PR. Macromolecules 1993;26:4144.
[17] Sundararajan PR, Kavassalis TA. J Chem Soc Faraday Trans 1995;91:2541.
[18] Yamamoto T. J Chem Phys 1997;107:2653.
[19] Takeuchi H. J Chem Phys 1998;109:5614.
[20] Sumpter BG, Noid DW, Liang GL, Wunderlich B. Adv Polym Sci 1994;116:73.
[21] Allen MP, Tildesley DJ. Computer simulation of liquids. Oxford, UK: Clarendon Press, 1987.
[22] Swope WC, Andersen HC, Berens PH, Wilson KR. J Chem Phys 1982;76:637.
[23] Gear CW. Report ANL 7126. Argonne National Laboratory, 1966.
[24] Rapaport DC. The art of molecular dynamics simulation. Cambridge, UK: Cambridge University Press, 1995.
[25] Liu C, Muthukumar M. J Chem Phys 1998;109:2536.
[26] Organ SJ, Keller A. J Mater Sci 1985;20:1602.
[27] Ungar G, Stejny J, Keller A, Bidd I, Whiting MC. Science 1985;229:386.
[28] Muthukumar M. Proc Natl Acad Sci USA 1999;96:11690.